IEEE Photonics Journal
An IEEE Photonics Society Publication

Open Access

Unusual Effect of Cerium Codoping on Stokes and Anti-Stokes Luminescence of BiOCl:Er^{3+} Crystal

Volume 7, Number 5, October 2015

Qun Liu
Yongjin Li
Qingliang Kuang
Zhiguo Song
Ronghua Wan
Yuting Zhou
Zuyuan Xu
Rui Hu
Jianbei Qiu
Zhengwen Yang
Zhaoyi Yin

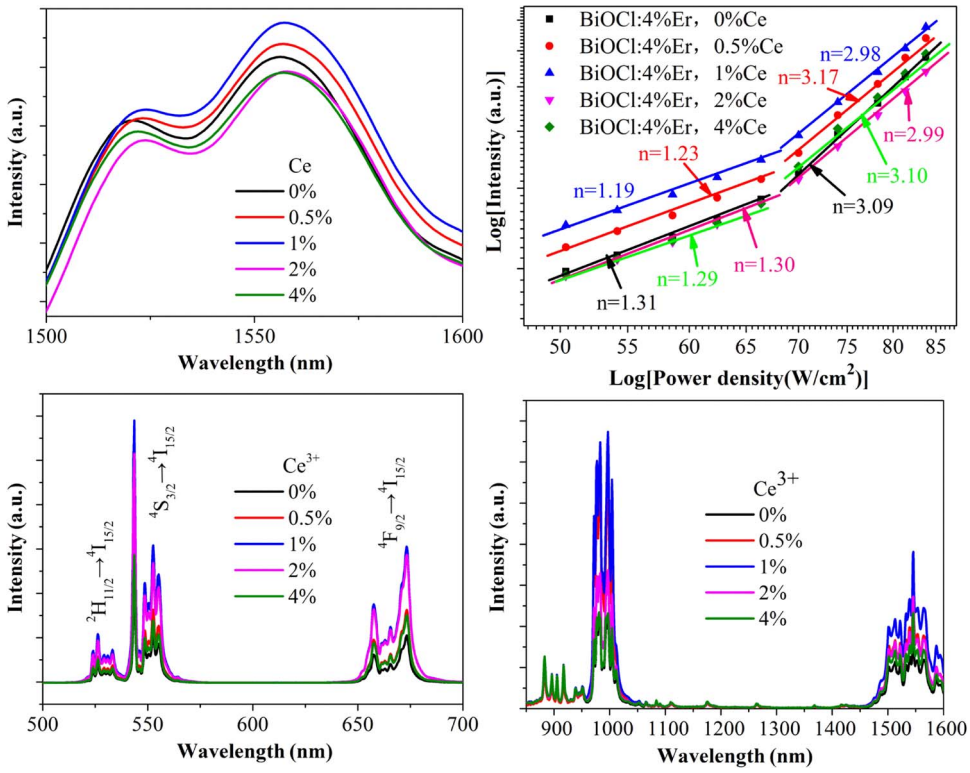

DOI: 10.1109/JPHOT.2015.2460115
1943-0655 © 2015 IEEE

Unusual Effect of Cerium Codoping on Stokes and Anti-Stokes Luminescence of BiOCl:Er^{3+} Crystal

Qun Liu,[1] Yongjin Li,[2] Qingliang Kuang,[1] Zhiguo Song,[1] Ronghua Wan,[1] Yuting Zhou,[1] Zuyuan Xu,[1] Rui Hu,[1] Jianbei Qiu,[1] Zhengwen Yang,[1] and Zhaoyi Yin[1]

[1]School of Materials Science and Engineering, Kunming University of Science and Technology, Kunming 650093, China
[2]Department of Science Research, Yunnan Technology and Business University, Kunming 651700, China

DOI: 10.1109/JPHOT.2015.2460115

Manuscript received June 24, 2015; revised July 19, 2015; accepted July 20, 2015. Date of publication August 20, 2015; date of current version August 27, 2015. This work was supported by the National Natural Science Foundation of China under Grant 61465006 and Grant 61265007. Corresponding author: Z. Song (e-mail: songzg@kmust.edu.cn).

Abstract: Effect of cerium codoping on Stokes or anti-Stokes luminescence of BiOCl:Er^{3+} crystals, which were controlled by a special photon avalanche (PA) mechanism under 980-nm excitation, was investigated. X-ray diffraction (XRD) and X-ray photoelectron spectroscopy (XPS) analysis indicate that Ce^{3+} ions were successfully doped into BiOCl lattices. However, in PA photoluminescence behaviors, the doped Ce^{3+} ions did not present efficient resonant energy transfer (ET) processes between the Er^{3+} ions as generally reported. As a result, the intensity of visible PA upconversion emission and 1.54 μm downshifting near-infrared (NIR) emission of Er^{3+} ions shows the same concentration dependence of cerium dopants. This phenomenon can be understood by the influence of cerium dopant content on the magnitude of internal electric field in layered BiOCl crystals, which may play a more important role on the upconversion (UC) and NIR luminescence of Er^{3+} than the traditional ET between rare-earth (RE) ions. The results of our work may offer a different understanding for the method to control the emissions of RE ions.

Index Terms: Ce–Er codoped, BiOCl crystals, photon avalanche, near-infrared (NIR) emission.

1. Introduction

Stokes or anti-Stokes luminescence of trivalent Er^{3+} ions doped in inorganic host have attracted extensive attention for applications such as lasers, biological imaging, infrared detection, and solar cells. [1]–[4] The 1.54 μm near infrared (NIR) emission of Er^{3+} which generally arises from a Stokes downshifted mechanism is particularly interesting as it can be used in eye-safe range-finding and optical fibers telecommunications [5]–[8]. However, the appearance of upconversion (UC) processes that convert the long-wavelength pump sources into short-wavelength emissions are generally believed to be losses for energy conversion into 1.54 μm emission. Therefore, resonant energy transfer processes through codoping Rare earth ions, such as cerium ion, is considered an efficient way to improve the 1.54 μm emission of Er^{3+} ions, because it generally can decrease the visible UC emission via enhancing the population feeding rate from the $^4I_{11/2}$ to the $^4I_{13/2}$ level of Er^{3+} [9], [10].

Alternatively, the generation of NIR emission is different with visible UC luminescence that shows high order power dependence. The population of the emitting level of 1.54 μm mostly depends on the relaxation from higher levels of Er^{3+} ions, such as $^4I_{11/2} \rightarrow {}^4I_{13/2}$ [11], which are excited by direct excited state absorption (ESA) or energy transfer (ET) from sensitized ions. Up to date, just few reports presented 1.54 μm emission of Er^{3+} formed through multi-photon process, which is generated by photon avalanche (PA) or similar PA mechanism [12], [13]. As for PA phenomena, it is a strongly non-linear process of population of an emitting high energy level of an active ion, which is considered as one of the relatively efficient one among three basic UC mechanisms but mostly observed in visible UC emissions of RE ions, such as Pr^{3+}, Ho^{3+}, Tm^{3+}, and Er^{3+} ions [14]–[17].

In previous work, we reported a hetero-looping enhanced energy transfer avalanche UC emission as well as synchronous downshifted NIR PA luminescence of Er^{3+} singly-doped BiOCl semiconductor poly-crystals, excited by a 980 nm laser [18]. According to energy level characteristic of Er^{3+} and Ce^{3+} ion and previous work on Ce^{3+}-Er^{3+} codoped material systems, it can be supposed that the Ce^{3+} doping may enhance the generation of metastable state reservoir level, $^4I_{11/2}$ levels, corresponding to 1.54 μm emission, which is benefit to get much more efficient NIR emission [5], [9], [10]. As far as we know, there has been no work on the effect of cerium doping on the NIR and visible PA emission of Er^{3+} ion.

In the present work, we reported the effect of CeO_2 dopants on PA Stokes or anti-Stokes luminescence of the special Er^{3+} doped semiconducting BiOCl crystals. However, results show that cerium doping can change the emission intensity of Er^{3+} but have no positive effect on the occurrence and looping property of the PA process. In particular, the visible UC emission and 1.54 μm emissions show the unusual synchronous dependence of cerium concentration, which is contrary to traditional luminescence behavior of Er-Ce codoped systems. The reason was discussed and the result may offer an all different understanding for material factor to control the emissions of RE ions.

2. Experimental

Samples of $Bi_{(1-x-0.04)}Er_{0.04}Ce_xOCl$ $(x = 0, 0.5, 1, 2, 4\ \mathrm{mol}\%)$ were prepared by solid state reaction. NH_4Cl (A.R.), Bi_2O_3 (99.99%), Er_2O_3 (99.99%), and CeO_2 (99.99%) were used as the starting materials. The weighed raw materials were thoroughly mixed in an agate mortar and then placed in a corundum crucible. Then, the powders were sintered at 500 °C for 3 h in air. Some excessive NH_4Cl (20%) is necessary for loss of Cl source at high temperature to obtain the pure phase formation.

The structure of the phosphors was recorded by X-ray diffraction (XRD) using Cu Kα radiation on a Bruker D8-Advance Diffractometer. The UV-vis-NIR absorption spectra of the samples were measured on a Hitachi U-4100 spectrophotometer. The valence state of doped Ce ion was detected using X-ray photoelectron spectroscopy (XPS). The UC emission spectra of the samples were measured using the Hitachi F-7000 Fluorescence Spectrophotometer with a 980 nm LD as excitation source. The downshifting NIR luminescence were measured using by a FLS980 fluorescence spectrophotometer (Edinburgh Instrument Ltd, UK) with Xe lamp as excitation as source (excitation wavelength 808 nm). The power dependence of NIR emission intensity were performed by a ZOLIX SBP300 spectrophotometer with InGAs as detector at 800–1800 nm under excitation of 980 nm laser diode (LD). All measurements were made at room temperature.

3. Results and Discussion

Fig. 1 presents the XRD patterns of the BiOCl:4% Er^{3+} powders codoped with Ce ions. As shown in Fig. 1(a), all the detectable peaks could be assigned to the tetragonal structure of BiOCl with space group of P4/nmm, which is in good agreement with the standard values for the BiOCl (JCPDS: No. 06-0249), indicating that pure phase BiOCl crystals have been synthesized successfully. The magnification of a selected region of diffraction peaks exhibits that the

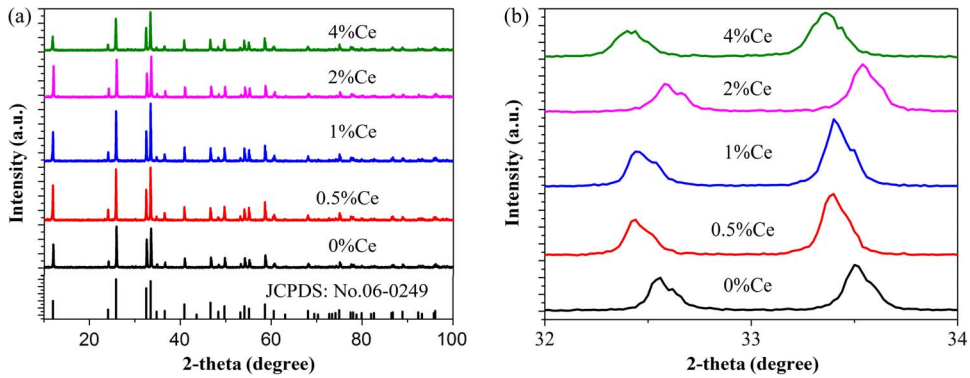

Fig. 1. (a) XRD patterns of BiOCl powders BiOCl:4% Er^{3+} powders codoped with Ce (0, 0.5, 1, 2, 4%). (b) Main diffraction peak near $2\theta = 32^\circ \sim 34^\circ$ with increasing Ce concentration.

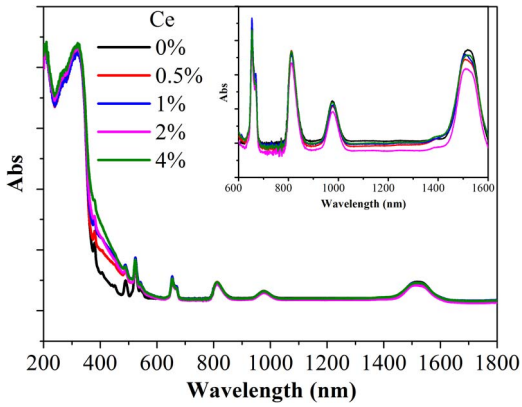

Fig. 2. UV-vis-NIR absorption of Ce doped BiOCl:Er^{3+} crystals.

diffraction peaks move to the small angle direction with increase of the Ce dopant concentration and subsequently move back to large angle direction when the Ce dopant concentration is over 1 mol% [see Fig. 1(b)]. It might because Ce ion might fill into the interstitial position of BiOCl crystals at low dopant concentration, and consequently the lattice size increase and the diffraction peak move to the small direction. In the case of high dopant level, Ce ions would begin to enter into the lattice of BiOCl crystals via substituting the position of Bi^{3+} ion. As a result, the lattice size decrease and the diffraction peak move to the large direction due to the smaller radius of Ce^{3+} or Ce^{4+} than Bi^{3+} [19], [20].

The UV-vis-NIR absorption of Er^{3+}-Ce codoped BiOCl is showed in Fig. 2. For semiconductor, changes in the optical properties are observed generally when impurity ions are doped in [21]. In the case of un-doped BiOCl, the intense absorption peak at about 330 nm along with an absorption edge rising steeply at about 378 nm is attributed to charge transfer from valence band (VB) to conduction band (CB) of BiOCl crystals. It shows that the absorption edge of samples Er^{3+}-Ce codoped BiOCl red-shifts gradually with the increase of Ce dopant concentration, further indicating effectively doping of Ce ions into BiOCl lattices.

However, the characteristic absorption peak of Ce^{3+} ion was not observed directly in the absorption spectra. To investigate the valence state of doped Ce ions, the representative XPS analysis of the samples doped 1% and 2% Ce was carried out. As showed in Fig. 3, the peaks of 911.45 eV, 899.28 eV, and 887.94 eV correspond to Ce^{4+} ions, and the peaks of 902.87 eV and 885.20 eV are ascribed to Ce^{3+} ion [22]. It indicates that Ce^{3+} ions are doped into BiOCl crystals. Therefore, the reason that typical absorption transitions of Ce^{3+} were not observed in the graph might because the absorption transitions of Ce^{3+} ions in BiOCl is in the

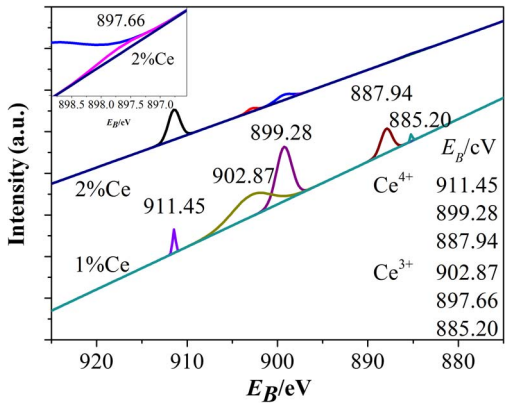

Fig. 3. Representative XPS analysis of the sample doped 1% and 2% Ce.

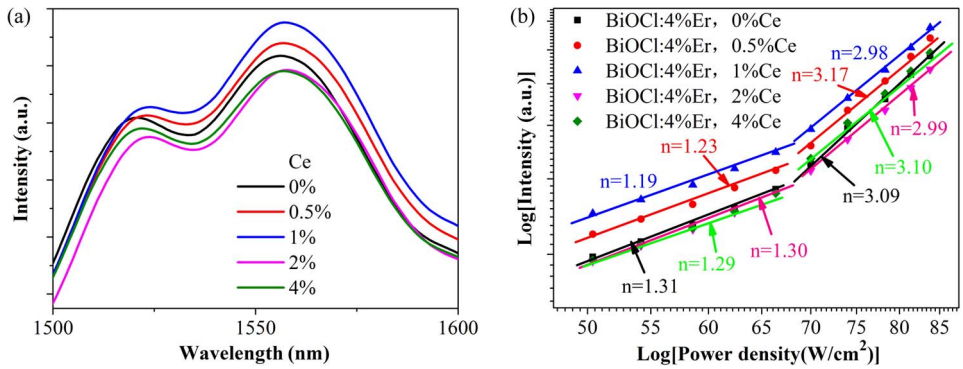

Fig. 4. (a) The 980 nm excited downshifted NIR fluorescence of prepared samples. (b) Plots of its corresponding pump power dependence.

ultraviolet region, which is overlapped with the intense absorption band of BiOCl semiconductor. On the other hand, according to peaks area calculation, the content ration of Ce^{3+}/Ce^{4+} was estimated to be about 0.73 and 0.108 for the sample doped 1% and 2% Ce, respectively. This indicates that Ce^{3+} ion is formed successfully and doped into BiOCl lattice, which is possibly due to reductive effect of NH4Cl atmosphere in high temperature solid reaction. It should be noted that the concentration of Ce^{3+} ions in BiOCl doped with 1% Ce is higher than the sample doped with 2% Ce, but the reason has not been understood well up to now.

Fig. 4 gives the downshifted NIR fluorescence of prepared samples excited by 980 nm and the plots of its corresponding pump power dependence. It shows that the intensity of 1.54 μm NIR emissions, ascribed the $(^4I_{13/2} \rightarrow {}^4I_{15/2})$ transition of Er^{3+} ion, was enhanced by Ce doping in low concentration, but was decreased when the Ce dopant concentration is more than 1% mole. Compared with the undoped sample, the luminescence intensity of sample doped with 1% Ce increased by 1.04 times. Interestingly, the pump power density dependence plots of NIR emission bands indicate that the 1.54 μm NIR luminescence present special PA emission behavior when the exaction power is over the threshold point [12]. It is well known that, for online emission processes, taking the UC luminescence as example, the photoluminescence intensity IUC depends on the pumping power IP according to the following equation [23]:

$$I_{UC} \propto I_p^n \tag{1}$$

where n is the number of pumping photons absorbed per UC photon emitted that can be easily calculated from the slope of the linear fit. For the special PA UC phenomena, the photon number

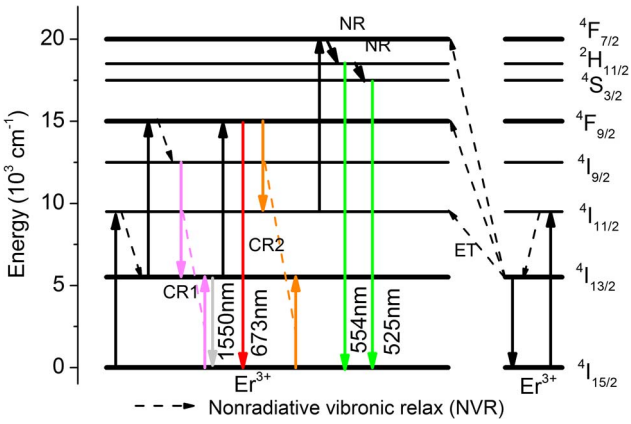

Fig. 5. Energy level diagram of Ce doped BiOCl:Er^{3+} crystals under excitation of 980 nm and the possible PA process.

n will increase sharply over the threshold point due to the occurrence of loping behavior. In this work, the NIR luminescence behaviors of obtained samples exhibit high order nonlinear emission like the UC process, when over power threshold point [see Fig. 4(b)].

The proposed mechanism of PA NIR emissions can be explained as Fig. 5. For the PA process, it is generally based on the existence of an efficient cross-relaxation (CR) process which can populate the intermediate state. We supposed that the $^4I_{13/2}$ level will become a dominant reservoir level through relaxation from $^4I_{11/2}$ level under the effect of intense internal polarized electric field as well as intense nonradiative vibration relaxation that is originated from the vibration of lattice and surface absorbed groups. The great enhancement of electron phonon interaction upon the threshold of excitation power can readily remedy the energy mismatch between the transitions with the intermediate energy level of Er^{3+} ion. Thus, the intermediate population of 4F9/2 level (red emission) and $^2H_{11/2}/^4S_{3/2}$ level (green emission) could were greatly enhanced and resulted in the occurrence of remarkable ratio between the population of reservoir level and the excited-state level, which initiated necessary condition for the UC PA processes and lead to the NIR PA behavior synchronously.

However, it should be noted that the Ce doping concentration can change the PA emission intensity but has no obvious either positive or positive effect on the occurrence and looping numbers of PA emission. In previous work, we found that the origin of PA emission was considered to be related to the special polarized internal electric field (IEF) in BiOCl crystals [24], which great improve the excitation ability of Er^{3+} ions through the enhancement effect of exciting field. Because the BiOCl crystallize in the tetragonal PbFCl structure (space group: P4/nmm; $Z = 2$) with alternating $(BiO)n^{n+}$ cation and Cl- anion layers, as showed in [24], which would induce the presence of strong IEF perpendicular to the $[Bi_2O_2]$ slabs and halogen anionic slabs in BiOCl. According to classic electrodynamics theory and our experiment result, the IEF of host will greatly influence the emission behavior of doped RE ions [25]. On the other hand, besides the PA emission behavior, the photon number of 1.54 μm NIR emission is slightly over 1 below the threshold point. This may be due to saturation effects of excited energy level that is also related to IEF in layered BiOCl crystals. Owing to indirect involvement to the aim of this work, the mechanism for these special phenomena will not be discussed in detail temporarily.

To better understand the effect of Ce dopant on the NIR emission intensity, the visible UC emission of the obtained samples was investigated as compared. Fig. 6 shows the visible UC emission spectral under excitation by 980 nm and the plots of its corresponding pump power dependence. The obtained samples exhibit characteristic sharp emissions, which can be attributed to $^2H_{11/2} \rightarrow {}^4I_{15/2}(\sim 525\ \text{nm})$, $^4S_{3/2} \rightarrow {}^4I_{15/2}(\sim 554\ \text{nm})$, and $^4S_{9/2} \rightarrow {}^4I_{15/2}(\sim 673\ \text{nm})$ transitions of Er^{3+} ions, respectively. Similar to that found in singly doped samples, the codoped crystals exhibit UC PA behavior, in which the number of UC photons (*n*) for green and red

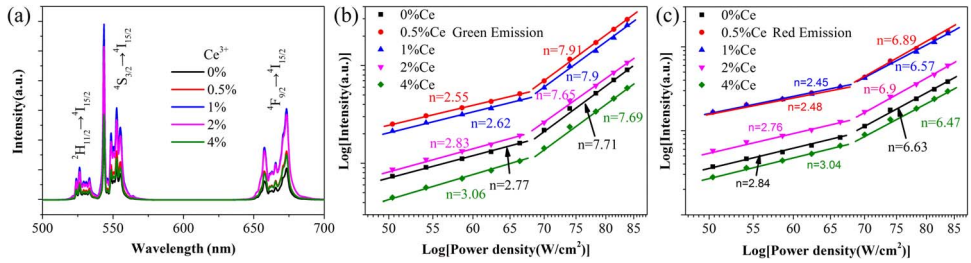

Fig. 6. (a) UC emission spectral of prepared samples under excitation at 980 nm. (b) Pump power dependence of the green emission. (c) Pump power dependence of the red emission.

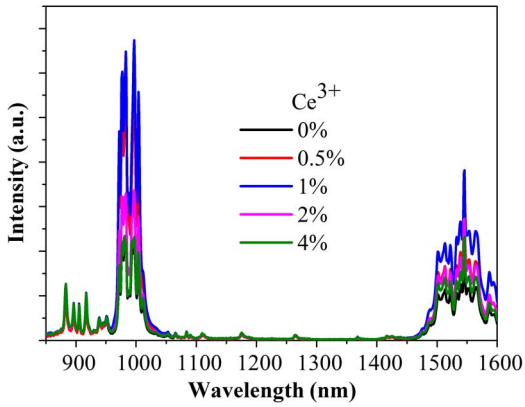

Fig. 7. Downshifted NIR luminescence of prepared samples excited by 808 nm.

emissions increase dramatically over the threshold of power density. It indicated that the possible number change of incident photons involved in the UC process caused by Ce doping was not obvious as that observed in downshifting NIR emission behaviors. However, the addition of Ce ions did not directly decrease the visible UC emission as previous reports [9], [22], [26]. In particular, the UC emissions show the synchronous concentration dependence of cerium dopant to that of 1.54 μm NIR emissions. This means that the enhancement of NIR emission caused by Ce doping is possibly not due to the traditional resonant energy transfer processes between Ce^{3+} and Er^{3+} ions.

Generally, the phonon-assisted energy transfer between Er^{3+} and Ce^{3+} would facilitate the population of the $^4I_{13/2}$ level and simultaneously reduces the UC process [9], [10]. To clarify the reason for unusual effect of cerium codoping on the Stokes or anti-Stokes luminescence of BiOCl:Er^{3+} crystals, the population state of $^4I_{11/2}$ energy level were studied by excitation at 808 nm. Fig. 7 gives the 808 nm exited downshifted NIR luminescence of prepared samples. It indicates that Er^{3+} ion emit special dominant 1 μm NIR emissions, meaning that the $^4I_{11/2}$ energy level of Er^{3+} ions doped in BiOCl may have greater emission cross area than in other crystals. This property of Er^{3+} doped BiOCl crystals may offer a new candidate for RE doped luminescent materials to getting efficient 1 μm NIR emission. However, result of NIR luminescence spectral clearly indicates that the concentration dependency of the NIR emission at 1 μm band on the Ce dopant is the same as that of visible UC emissions, as well as 1.54 μm NIR emissions. Namely, without luminescence lifetime analysis, the above results clearly indicate that the doping of Ce^{3+} ions do not improve the relaxation of $^4I_{11/2} \rightarrow {}^4I_{13/2}$, or the resonant energy transfer processes between Er^{3+} and Ce^{3+} ions is not the crucial factor that determined UC and 1.54 μm NIR emission process in BiOCl crystals.

It is worth noting that with the increase of Ce addition, the change trend of PA luminescence of BiOCl:Er^{3+} crystals is closely related to that of the XRD results. That is, considering the effect of Ce dopant concentration, the turning point for the two kinds of properties is synchronous.

This means that the luminescence intensity of Er^{3+} ions in BiOCl crystals is more possibly determined by material structure rather than by energy transfer between RE ions. In previous work, we found that the magnitude of IEF in BiOCl play a crucial role on occurrence of the PA emission mechanism and luminesce intensity of Er^{3+} ion because according to classic electrodynamics theory [27], the intensity of photoluminescence, especially the high order nonlinear photoluminescence, is greatly involved with the IEF of the host. Therefore, the unusual effect of Ce doping on the Stokes or anti-Stokes PA luminescence of BiOCl:Er^{3+} crystals might be explained as follows. Ce^{4+} ion has smaller a radius and can enter into the interstitial sites when doped into BiOCl crystals, which may form cation vacancy and charge disequilibrium in lattice. This would decrease the magnitude of IEF, which play a more important role on the PA emission intensity than the Ce^{3+} ion. Therefore, the samples containing more Ce^{4+} ions may present relatively lower emission intensity, such as the BiOCl:Er^{3+} doped with 1 and 2% Ce. Although it has no effective method to quantitatively analyze the variation of IEF in BiOCl crystals up to date, this work may offer a different insight into the material structure factor that determines and controls the photoluminescence of doped RE ions.

4. Conclusion

Ce ion can be doped into BiOCl:Er^{3+} semiconducting crystals, but Ce^{3+} did not act as efficient resonant ions to change the visible UC emission and 1.54 μm NIR luminesce of Er^{3+} ion as it did previously. The unusual effect of cerium codoping on Stokes and anti-Stokes PA luminescence of BiOCl:Er^{3+} crystals may be understood by cerium dopant content on the magnitude of IEF in layered BiOCl crystals, which play a more important role on the Er^{3+} activated luminescence.

References

[1] Y. Liu, D. Tu, H. Zhu, and X. Chen, "Lanthanide-doped luminescent nanoprobes: Controlled synthesis, optical spectroscopy, and bioapplications," *Chem. Soc. Rev.*, vol. 42, pp. 6924–6958, 2013.

[2] F. Auzel, "Upconversion and anti-stokes processes with f and d ions in solids," *Chem. Rev.*, vol. 104, no. 1, pp. 139–174, 2004.

[3] G. Chen, H. Qiu, P. N. Prasad, and X. Chen, "Upconversion nanoparticles: Design, nanochemistry, and applications in theranostics," *Chem. Rev.*, vol. 114, no. 10, pp. 5161–5214, 2014.

[4] J. Boyer, L. A. Cuccia, and J. A. Capobianco, "Synthesis of colloidal upconverting $NaYF_4$:Er^{3+}/Yb^{3+} and Tm^{3+}/Yb^{3+} monodisperse nanocrystals," *Nano Lett.*, vol. 7, no. 3, pp. 847–852, 2007.

[5] B. Simondi-Teisseire *et al.,* "Room-temperature CW laser operation at ~1.55 μm (eye-safe range) of Yb:Er and Yb:Er:Ce:Ca2Al2SiO7 crystals," *IEEE J. Quantum Electron.*, vol. 32, no. 11, pp. 2004–2009, Nov. 1996.

[6] S. Trpkovski, D. J. Kitcher, G. W. Baxter, S. F. Collins, and S. A. Wade, "High-temperature-resistant chemical composition Bragg gratings in Er^{3+}-doped optical fiber," *Opt. Lett.*, vol. 30, no. 6, pp. 607–609, Mar. 2005.

[7] Y. Zhao *et al.,* "Homogeneity of bismuth-distribution in bismuth-doped alkali germanate laser glasses towards superbroad fiber amplifiers," *Opt. Exp.*, vol. 23, no. 9, pp. 12423–12433, May 2015.

[8] X. Liu *et al.,* "Optical gain at 1550 nm from colloidal solution of Er^{3+}-Yb^{3+} codoped $NaYF_4$ nanocubes," *Opt. Exp.*, vol. 17, no. 7, pp. 5885–5890, Mar. 2009.

[9] E. Sani, A. Toncelli, and M. Tonelli, "Spectroscopy of Ce-codoped Er:BaY_2F_8 single-crystals," *Opt. Mater.*, vol. 28, no. 11, pp. 1317–1320, Aug. 2006.

[10] J. Dong *et al.,* "Dual-pumped tellurite fiber amplifier and tunable laser using Er/Ce codoping scheme," *IEEE Photon. Technol. Lett.*, vol. 23, no. 11, pp. 736–738, Jun. 2011.

[11] X. Gong *et al.,* "Spectral properties and 1.55 μm laser operation of Ce^{3+}:Yb^{3+}:Er^{3+}:$NaLa(WO_4)_2$ crystal," *J. Appl. Phys.*, vol. 108, no. 7, 2010, Art. ID. 073524.

[12] G. Chen *et al.,* "Generation of 1.5 μm emission through an upconversion-mediated looping mechanism in Er^{3+}/Sc^{3+}-codoped LiNbO3 single crystal," *Opt. Lett.*, vol. 37, no. 7, pp. 1268–1270, Apr. 2012.

[13] G. Chen, H. Liang, H. Liu, G. Somesfalean, and Z. Zhang, "Anomalous power dependence of upconversion emissions in Gd_2O_3:Er^{3+} nanocrystals under diode laser excitation of 970 nm," *J. Appl. Phys.*, vol. 105, 2009, Art. ID. 114315.

[14] M. Joubert, "Photon avalanche upconversion in rare earth laser materials," *Opt. Mater.*, vol. 11, no. 2/3, pp. 181–203, Jan. 1999.

[15] J. S. Chivian, W. E. Case, and D. D. Eden, "The photon avalanche: A new phenomenon in Pr^{3+}-based infrared quantum counters," *Appl. Phys. Lett.*, vol. 35, no. 2, pp. 124–125, Jul. 1979.

[16] B. C. Collings and A. J. Silversmith, "Avalanche upconversion in LaF_3:Tm^{3+}," *J. Luminescence*, vol. 62, no. 6, pp. 271–279, Dec. 1994.

[17] X. Wang, S. Xiao, Y. Bu, X. Yang, and J. W. Ding, "Visible photon-avalanche upconversion in Ho^{3+} singly doped β-Na $(Y_{1.5}Na_{0.5})F_6$ under 980 nm excitation," *Opt. Lett.*, vol. 33, no. 22, pp. 2653–2655, Nov. 2008.

[18] Y. Li *et al.,* "High multi-photon visible upconversion emissions of Er^{3+} singly doped BiOCl microcrystals: A photon avalanche of Er^{3+} induced by 980 nm excitation," *Appl. Phys. Lett.*, vol. 103, no. 23, 2013, Art. ID. 231104.
[19] Y. Bai *et al.,* "The effect of Li on the spectrum of Er^{3+} in Li-and Er-codoped ZnO nanocrystals," *J. Phys. Chem. C*, vol. 112, no. 32, pp. 12259–12263, 2008.
[20] Y. Bai *et al.,* "Enhanced upconverted photoluminescence in Er^{3+} and Yb^{3+} codoped ZnO nanocrystals with and without Li^{+} ions," *Opt. Commun.*, vol. 281, no. 21, pp. 5448–5452, Nov. 2008.
[21] M. Pal, U. Pal, J. M. G. Y. Jiménez, and F. Pérez-Rodríguez, "Effects of crystallization and dopant concentration on the emission behavior of TiO_2 : Eu nanophosphors," *Nanoscale Res. Lett.*, vol. 7, pp. 1–12, 2012.
[22] F. B. Li, X. Z. Li, M. F. Hou, K. W. Cheah, and W. Choy, "Enhanced photocatalytic activity of Ce^{3+}-TiO_2 for 2-mercaptobenzothiazole degradation in aqueous suspension for odour control," *Appl. Catalysis A: Gen.*, vol. 285, no. 1/2, pp. 181–189, May 2005.
[23] S. Xiao, X. Yang, J. W. Ding, and X. H. Yan, "Up-conversion in Yb^{3+}-Tm^{3+} co-doped lutetium fluoride particles prepared by a combustion–fluorization method," *J. Phys. Chem. C*, vol. 111, no. 23, pp. 8161–8165, 2007.
[24] L. Zhang, W. Wang, S. Sun, D. Jiang, and E. Gao, "Selective transport of electron and hole among {001} and {110} facets of BiOCl for pure water splitting," *Appl. Catalysis B: Environ.*, vol. 162, pp. 470–474, Jan. 2015.
[25] Y. Li *et al.,* "Far-red-emitting BiOCl:Eu^{3+} phosphor with excellent broadband NUV-excitation for white-light-emitting diodes," *J. Amer. Ceramic Soc.*, vol. 98, no. 7, pp. 2170–2176, Jul. 2015.
[26] Y. H. Tsang, D. J. Binks, B. Richards, and A. Jha, "Spectroscopic and lasing studies of Ce^{3+}:Er^{3+}:Yb^{3+}:YVO_4 crystals," *Laser Phys. Lett.*, vol. 8, no. 10, p. 729, 2011.
[27] J. Wang, M. S. Gudiksen, X. Duan, Y. Cui, and C. M. Lieber, "Highly polarized photoluminescence and photodetection from single indium phosphide nanowires," *Science*, vol. 293, no. 5534, pp. 1455–1457, Aug. 2001.